Nucleotide Effects on the Structure and Dynamics of Actin

Xiange Zheng, Karthikeyan Diraviyam, and David Sept
Center for Computational Biology and Department of Biomedical Engineering, Washington University, St. Louis, Missouri 63130

ABSTRACT Adenosine 5′-triphosphate or ATP is the primary energy source within the cell, releasing its energy via hydrolysis into adenosine 5′-diphosphate or ADP. Actin is an important ATPase involved in many aspects of cellular function, and the binding and hydrolysis of ATP regulates its polymerization into actin filaments as well as its interaction with a host of actin-associated proteins. Here we study the dynamics of monomeric actin in ATP, ADP-P_i, and ADP states via molecular dynamics simulations. As observed in some crystal structures we see that the DNase-I loop is an α-helix in the ADP state but forms an unstructured coil domain in the ADP-P_i and ATP states. We also find that this secondary structure change is reversible, and by mimicking nucleotide exchange we can observe the transition between the helical and coil states. Apart from the DNase-I loop, we also see several key structural differences in the nucleotide binding cleft as well as in the hydrophobic cleft between subdomains 1 and 3 where WH2-containing proteins have been shown to interact. These differences provide a structural basis for understanding the observed differences between the various nucleotide states of actin and provide some insight into how ATP regulates the interaction of actin with itself and other proteins.

INTRODUCTION

Actin is one of the most abundant proteins in eukaryotic cells and it is essential for numerous cellular functions. Monomeric or G-actin polymerizes in a polar fashion to form actin filaments or F-actin, and it is primarily these filaments that participate in processes such as cell motility, transport, and cytokinesis. Although actin can be polymerized in the nucleotide-free state (1), the binding of adenosine 5′-triphosphate or ATP and subsequent hydrolysis into adenosine 5′-diphosphate or ADP is known to be a critical factor in controlling the interaction of actin both with itself and with other proteins. In terms of polymerization, ATP-actin polymerizes faster and dissociates slower than ADP-actin, at both the fast growing barbed end as well as the slower growing pointed end (2). Once it is polymerized, ATP is hydrolyzed with a half time of 2 s, and the inorganic phosphate remains trapped in the nucleotide site for several minutes before being released (2–4). As such, there are three distinct regions of the actin filament: an ATP region near the growing tip of the filament, an intermediate ADP-P_i domain where the phosphate is retained, and an ADP region in the central portion of the filament. There is structural evidence that the different nucleotide states of the filament have slightly different conformations (5), and it has been well established that several F-actin-binding proteins preferentially interact with one or more of these states of the filament. The Arp-2/3 complex binds 25-fold better to ATP filaments than to ADP filaments (6), a property that would naturally enhance Arp-2/3 complex mediated branching at the leading edge of the cell and restrict binding and branching farther away from the area of active actin polymerization. Similarly, proteins of the ADF/cofilin family have been shown to bind 10–50-fold better to ADP-actin as compared to the ATP state of the filament (7,8). This would likewise help restrict the severing activity of these proteins to older regions of the actin filament network. In terms of monomeric or G-actin, profilin aids in actin nucleotide exchange and binds stronger to monomeric actin in the ATP state (9,10). Proteins that bind to G-actin through a WH2 domain (such as proteins of the SCAR/WASp family, MIM, or thymosin-β4) have also been shown to preferentially bind to ATP-actin, a feature that is likely key for their function in recruiting polymerization-competent monomers (11–14). Although the biochemistry and thermodynamics have been well characterized, the structural basis for this binding selectivity has not been determined.

There is significant structural data on actin, a 375-amino-acid protein consisting of four subdomains surrounding a nucleotide binding cleft (see Fig. 1). The first crystal structure of monomeric actin was obtained as a cocrystal with DNase-I (15), and since this time >40 crystal and cocrystal structures have been solved. There are inherent difficulties in crystallizing actin as an unmodified monomer since its strong tendency is to polymerize; however, through covalent modification with tetramethylrhodamine (TMR), the Dominguez lab was able to obtain structures for both the ADP and ATP states of actin (16,17). These structures revealed some differences between the two nucleotide states, the most prominent feature being that the DNase-I loop (hereafter referred to as the D-loop) formed a regular α-helix in the ADP state but was unstructured to the point of not being resolved in the ATP state. Recently Rould et al. crystallized a nonpolymerizing actin mutant in both nucleotide states and found the D-loop to be in a coil conformation in both crystals (18). They attributed the differences observed with TMR-modified actin to be a result of crystal contacts and concluded that the

Submitted March 19, 2007, and accepted for publication April 25, 2007.

Address reprint requests to David Sept, Biomedical Engineering, Campus Box 1097, Washington University, St. Louis, MO 63130-4899. Tel.: 314-935-8837; Fax: 314-935-7448; E-mail: dsept@biomed.wustl.edu.

Editor: Steven D. Schwartz.

0006-3495/07/08/1277/07 $2.00

doi: 10.1529/biophysj.107.109215

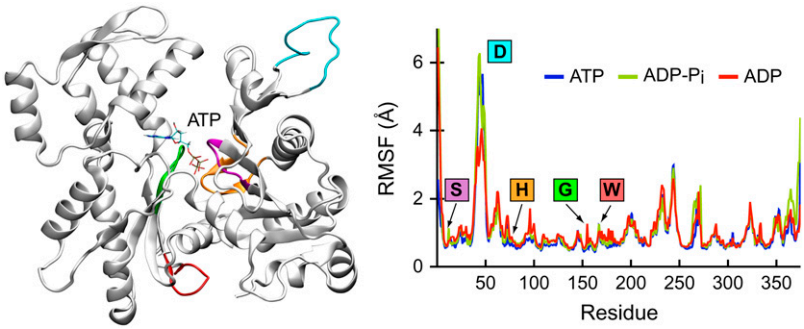

FIGURE 1 Four-domain structure of the actin monomer (*left*) and the observed RMSFs over the 50-ns simulations (*right*). Highlighted are the S-loop (*purple*), D-loop (*cyan*), H-loop (*apricot*), G-loop (*green*), and W-loop (*red*).

D-loop was inherently nonhelical. Apart from the D-loop, these crystallographic structures revealed several other portions of the actin monomer that were nucleotide dependent. These include the H-loop—the region from 70–78 that contains the methylated histidine at position 73—and the S-loop—the stretch of residues 11–16 that includes Ser-14 (16,17,19).

Here, through the use of multiple, long molecular dynamics (MD) simulations we present details on the conformation and dynamics of G-actin in the ATP, ADP-P_i, and ADP states. These types of simulations hold significant advantages in studying such problems since we are able to work with unmodified, wild-type actin in the monomeric state without any concerns about polymerization or other interactions. Our results show clear differences between these three nucleotide states and provide strong evidence for how these states regulate the interaction of actin with itself and with actin-associated proteins.

METHODS

Preparation of protein structures

The starting structures for the simulations of ATP-actin and ADP-actin were taken from the protein data bank (IDs: 1NWK and 1J6Z, respectively). The bound metal ions and water molecules from the original crystal structures were included, where the calcium ion was replaced with magnesium and the nonhydrolyzable nucleotide in the 1NWK structure replaced with ATP. To replace the missing DNase-I binding loop (residues 40–51) in ATP-actin, we first fit the ADP and ATP crystal structures using all common backbone atoms and then grafted the missing portion from ADP-actin to ATP-actin. The PLOP program (20) was used to complete the two structures by adding missing heavy atoms and hydrogens and minimizing the stretched bonds from the grafting procedure. The protonation state of histidine residues was assigned using the pdb2gmx module of the GROMACS package (21). For the ADP-P_i structure, the same procedure was used as for ATP, but the bond between the β-phosphate oxygen in the ADP segment and the γ-phosphate was broken and the phosphate group was protonated.

Molecular dynamics simulations

The MD simulations of the three systems were undertaken with period boundary conditions using the NAMD simulation package version 2.6b1 (22). For each system, 12 Å of water was added to solvate the protein, and counterions Na^+ and Cl^- were added to neutralize the system and give an ionic strength of 40 mM. Particle mesh Ewald (PME) (23) was used for long-range electrostatics interactions, and all-atom CHARMM22 and CHARMM27 force fields (24) as well as the TIP3P water model (25) were employed. The parameters and settings used in the simulations are as follows: 1), the isothermal-adiabatic ensemble (NPT) at 1 atm pressure, using the Nosé-Hoover Langevin piston (26) with a decay period of 200 fs (damping timescale of 100 fs for heating and equilibration phases and 500 fs for production phase); 2), a bond interactions calculation frequency of 2 fs, short-range electrostatics and van der Waals interactions frequency of 2 fs, with 10.0 Å as cutoff and 8.5 Å as smooth switching; and 3), long-range computing frequency of 4 fs, with PME grid points at least 1 Å in all directions. The MD simulations were carried out in the following steps: minimization of the system down to 0.01 kcal/mol gradient; C_α restrained heating to 300 K in 75 K intervals and equilibration for 80 ps; with C_α restraints removed, equilibration of the system for 600 ps; production run of 75 ns for ATP-actin, 50 ns for ADP-P_i, and 50 ns for ADP-actin. To eliminate any artifacts from using the D-loop from ADP-actin, the first 25 ns of trajectories was ignored; however, this portion of the simulation did provide the helix-coil transition we observed.

Data analysis and visualization

Most analysis, in particular the secondary structure assignment shown in Figs. 2–5, was carried out using the analysis tools included in the GROMACS package (21). All molecular images were produced with visual molecular dynamics (27).

RESULTS

Having structures for ATP-actin, ADP-actin, and ADP-P_i-actin, we performed three separate 50-ns MD simulations with explicit water and ions (see Supplementary Material for movies of trajectories). Actin is often functionally divided into four subdomains, which span the following residues: subdomain 1 (residues 1–32, 70–144, and 338–375), subdomain 2 (residues 33–69), subdomain 3 (residues 145–180 and 270–337), and subdomain 4 (residues 181–269). Using the average ATP-actin structure from our simulations as a reference and aligning the structures using only subdomains 3 and 4, the average structures of ADP-actin and ADP-P_i-actin had backbone root mean-square deviation (RMSD) values 2.1 Å and 2.0 Å, respectively. When just the backbone of subdomains 3 and 4 was used, this RMSD fell to 0.7 Å in both cases, indicating that these subdomains of the protein do not experience a significant conformational shift. To look for global shifts in the arrangement of these subdomains, we calculated the center of mass distances between these subdomains (using C_α positions) over the course of the simulations. This is a relatively coarse-grained method of

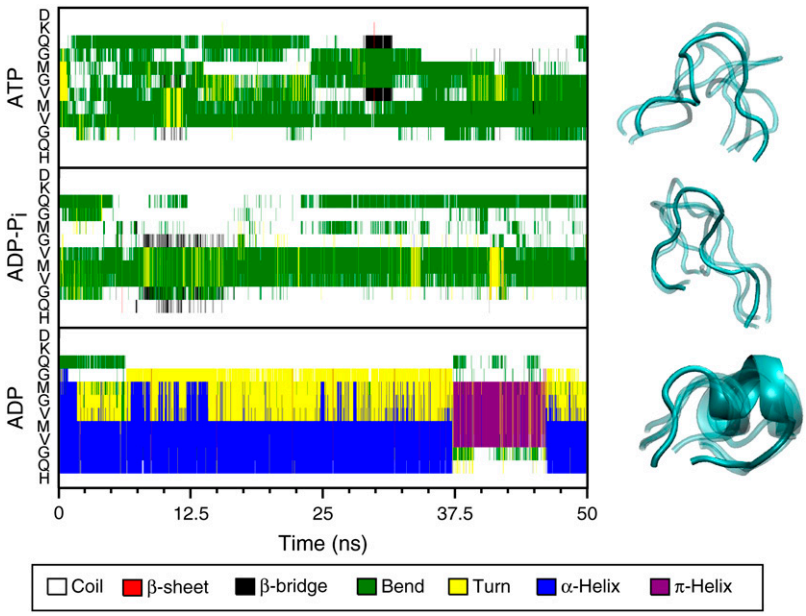

FIGURE 2 Secondary structure of the D-loop in the ATP, ADP-P_i, and ADP states over the 50-ns simulations. The colors indicate the secondary structure for each residue at each time point (see legend) and the order of residues in each panel is from H-40 on the bottom to D-51 at the top. The structures depicted on the right are taken at 10-ns intervals over the course of the simulation.

assessing conformational changes within the actin monomer, but it did reveal that subdomains 1 and 3 are slightly closer together in the ADP state than in the ATP or ADP-P_i states (24.7 ± 0.3 Å vs. 25.5 ± 0.2 Å). The other subdomain distances were similar in all three nucleotide states. Just like the static conformations, the dynamics and relative motions of each actin state were largely conserved, the largest root mean-square fluctuation (RMSF) deviations being small differences in the movement of the D-loop (see Fig. 1). The C- and N-termini also displayed similar mobility in all three nucleotide states, although some minor differences in the movement of the C-terminus were evident. Apart from the D-loop, other surface loops, including the subdomain 3/4 loop and hydrophobic plug, showed significant dynamics, but there again were no discernable differences between the ATP, ADP-P_i, and ADP simulations.

Although global analysis of the actin structures did not reveal significant changes in conformation (RMSD) or dynamics (RMSF), there are several localized regions that show a specific conformational dependence on the state of the nucleotide. As highlighted in Fig. 1, these include the D-loop (defined as residues 40–51), the H-loop (residues 70–78) containing the methylated histidine at position 73, the W-loop (residues 165–172) where WH2 domain containing proteins bind, and several regions in the nucleotide binding cleft including the S-loop (residues 11–16) and the G-loop (residues 154–161). Below we present the results for each of these individual regions.

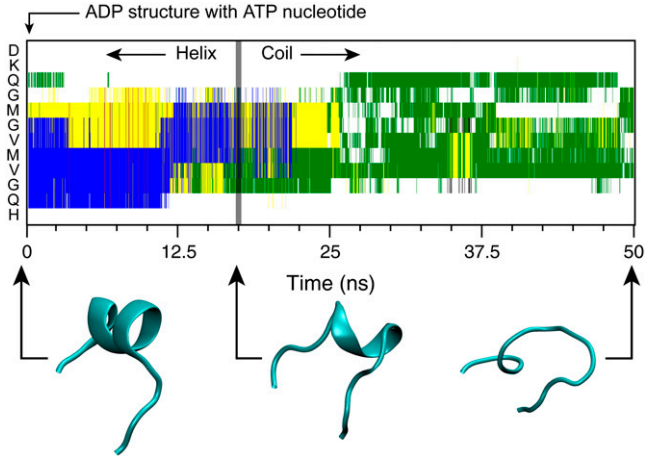

FIGURE 3 Helix-coil transition observed in the D-loop. This simulation was started with ATP monomer structure but with the D-loop in the helical/ADP conformation (see text for details). See Fig. 2 for the color legend explaining the secondary structure.

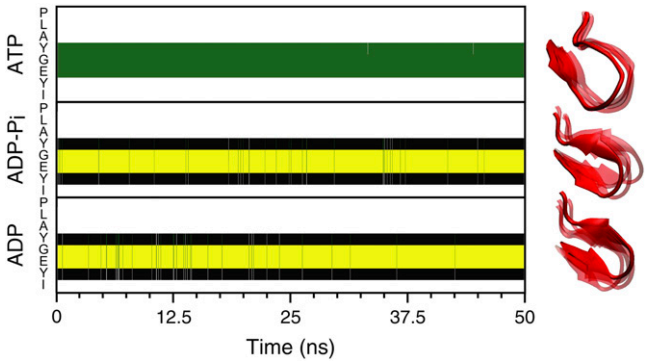

FIGURE 4 Secondary structure of the W-loop in the ATP, ADP-P_i, and ADP states over the 50-ns simulations. The colors indicate the secondary structure for each residue at each time point (see Fig. 2 for legend). The residue order goes from I-165 (*bottom*) to P-172 (*top*) in each panel. The structures depicted on the right are taken at 10-ns intervals over the course of the simulation.

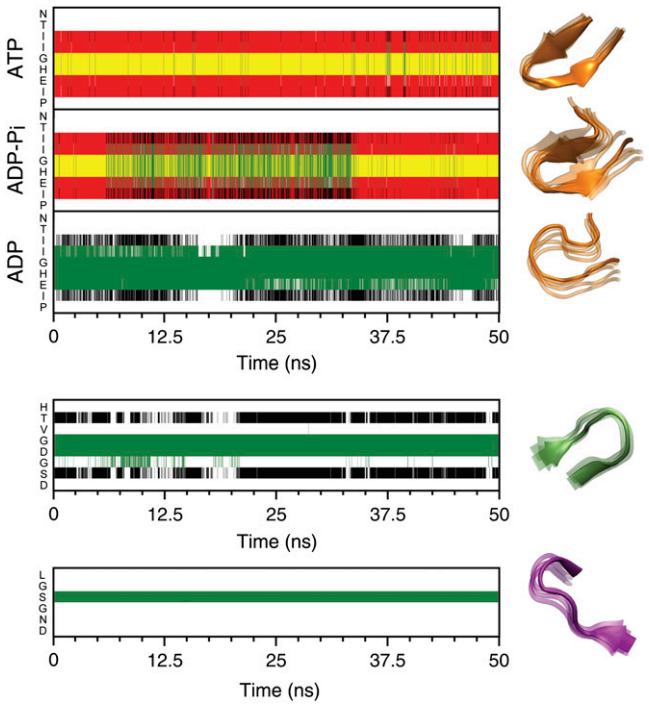

FIGURE 5 Secondary structures of the H-loop (*top*), G-loop (*middle*), and S-loop (*bottom*) over the 50-ns simulations. Since the G-loop and S-loop were identical in all three nucleotide states, only the ATP state is shown. The colors are the same as in Fig. 2 and the structures depicted on the right are taken at 10-ns intervals over the course of the simulation. The residue order goes from (*bottom* to *top*): P-70–N-78 for the H-loop, D-154–H-161 for the G-loop, and D-11–L-16 for the S-loop.

The DNase-I binding loop

Fig. 2 shows the secondary structure of the D-loop for ATP-actin, ADP-P_i -actin, and ADP-actin over the 50-ns time course of each simulation. We observe clear differences in the three-nucleotide states, with the D-loop forming a stable α-helix in the ADP state but adopting a coil conformation in both the ATP and ADP-P_i states. The dependence of the D-loop on the nucleotide state has been a point of disagreement, and it has been suggested that the helix observed in the ADP state was a result of crystallization and did not reflect an intrinsic property of the protein (18,28). To test this hypothesis, we performed a simple test where we started with the ADP D-loop structure (i.e., an α-helix) on the ATP monomer, in a sense mimicking the conformation after nucleotide exchange. In this case, the D-loop remained helical for ~18 ns, after which it transitioned to a coil state where it remained for a further 50 ns (Fig. 3 and Supplementary Material). Contrast this with the result from the ADP simulation where the helix remained stable for >50 ns (Fig. 2), and it strongly suggests that the secondary structure of the D-loop is nucleotide dependent; however, since we have only observed single transition, we cannot state this more definitively. It seems most probable that both conformations are present in any of the nucleotide states, and hydrolysis and/or phosphate loss simply shifts the equilibrium balance between the coil and helix states.

The W-loop

Residues 154–161 in subdomain 3 are the prime interaction point for WH2 domains in proteins such as the SCAR/WASp family and other WH2-containing proteins like thymosin-β4. As shown in Fig. 4, we see this region change from coil in the ATP state to β-sheet in the ADP-P_i and ADP states. This subtle change is the result of a backbone hydrogen bond between Y-166 and Y-169, a canonical $(n,n+3)$ β-turn, and these structures are stable in all three simulations over the entire 50 ns. There is evidence that WH2-containing proteins preferentially interact with ATP-actin over ADP-actin (12, 13,29) presumably as a method of ensuring the fastest rate of nucleation or polymerization. Since this region shows a unique ATP conformation it seems likely that this is the structural basis for this selectivity; however, more simulation and experimental studies will be required to fully explore this issue.

The nucleotide-binding cleft

The loop containing the methylated H-73 spans residues 70–78 and was denoted a sensor loop by Graceffa and Dominguez (17). As shown in Fig. 5, this loop adopts different conformations in the three-nucleotide states of actin. In ATP-actin, the H-loop forms a β-sheet, with stabilizing hydrogen bonds formed between backbone atoms from P-70 to T-77 and E-72 to I-75 as well as side-chain interactions between E-72 and T-77 (see Fig. 6 for details). In the ADP-P_i -actin, the H-loop adopts a similar β-sheet conformation, forming the identical hydrogen bonds as in the ATP state. In the case of ADP-actin the H-loop loses most of its hydrogen-bonding network and forms an unstructured coil. As observed in Fig. 6, P-70 still interacts with T-77, but the other bonds, in particular the E-72-I-75 backbone interaction, are broken and replaced with solvent interactions. In addition to the H-loop, the S-loop and G-loop help provide the intrinsic structure of the nucleotide-binding site. The S- and G-loops contain S-14 and G-158, respectively, two residues that are highly conserved in NTPases and have direct interactions with the nucleotide (30). These two loops form β-hairpins in the ADP and ATP crystal structures of both TMR-modified and mutant actins (16–18,31), and we observe no deviations from these structures. Fig. 5 shows the secondary structures of these loops over the time course of the ATP simulation, but the plots for the ADP-P_i and ADP simulations were indistinguishable and are not shown.

One distinct advantage of MD simulations is the ability to observe and analyze atomic-level interactions. Fig. 6 shows details of the nucleotide-binding site in all three nucleotide states of actin. In ATP-actin, there are several interactions between the H-, S-, and G-loops. The backbone amide and

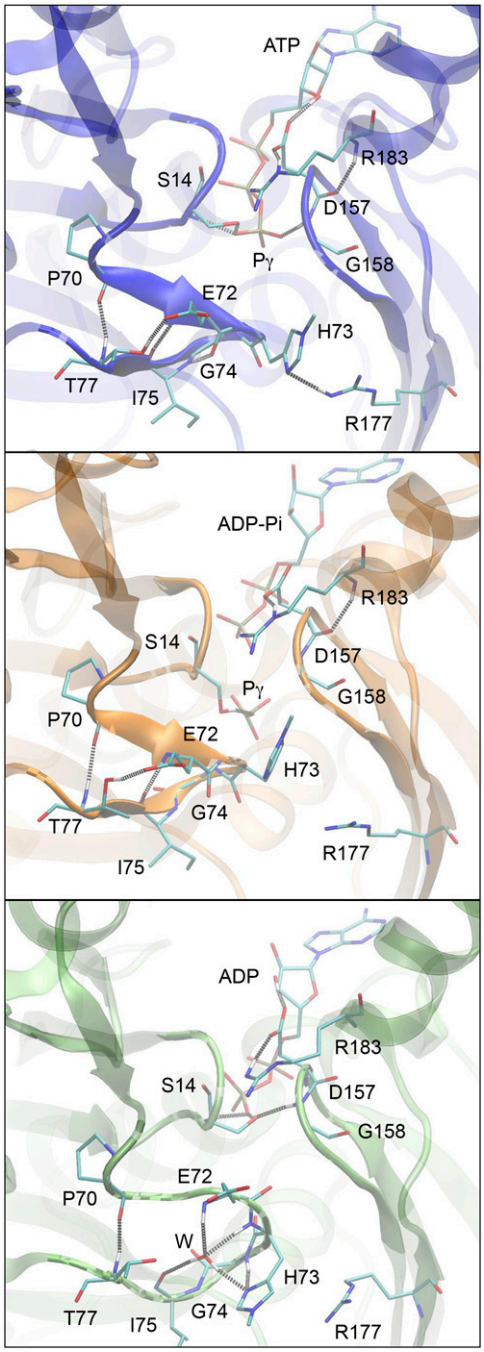

FIGURE 6 Details of the nucleotide-binding site in the ATP, ADP-P_i, and ADP states. The interactions between the nucleotide and the surrounding loops as well as other key residues on the H-, S-, and G-loops are highlighted. For clarity, water molecules and hydrogens are only shown for interacting residues and hydrogen bonds are depicted as dashed lines.

γ-oxygen of S-14 form hydrogen bonds with ATP, whereas another γ-oxygen of ATP hydrogen bonds with the backbone amide of G-158 on the G-loop. In this sense, ATP serves as a bridge connecting the S- and G-loops, as in many NTPases (30). R-183 has two interactions with D-157, through both side chain and backbone hydrogen bonds, and also bonds to I-71 on the H-loop via a bridging water molecule. Finally at the bottom of the binding cleft, the δ-nitrogen of H-73 interacts with the side chain of R-177 on the opposite side of the binding cleft. When considered as a whole, this network of hydrogen bonds links together the S-loop, H-loop, and G-loop, holding the nucleotide-binding cleft in a closed conformation. The interactions for ADP-P_i actin are similar to those in ATP-actin. S-14 now interacts with P_i, but since the γ-phosphate is now dissociated, it is not close enough to interact directly with ADP. The interaction between ATP and G-158 is now replaced with two water-mediated interactions between ADP and P_i, and P_i and G-158 (see Fig. 6), and the bond between H-73 and R-177 is now bridged by water molecules. Finally for ADP-actin, as a consequence of phosphate loss, residue S-14 moves closer to both the terminal β-oxygen of ADP and the G-loop, interacting simultaneously with both ADP and G-158. The direct interaction between residues S-14 and G-158 emphasizes the shorter distance between S- and G-loops, supporting the finding that these two loops move slightly closer together upon hydrolysis and phosphate dissociation (18).

DISCUSSION

The hydrolysis of ATP is the primary source of energy within the cell, and although ATP does affect the polymerization behavior of actin, it appears that in the case of actin ATP plays a more important role as a timekeeper, demarcating newly polymerized regions from older portions of the filament (32). Via this simple mechanism, the binding of proteins such as the Arp-2/3 complex is concentrated near the growing barbed end of the filament that is predominantly ATP, and proteins like ADF and cofilin are primarily found in ADP-rich regions of the filament. Although there is no apparent need for such a timing mechanism for G-actin, it is important for many actin-binding proteins to discriminate between the various nucleotide states of actin. This is certainly the case for WH2-containing proteins such as N-WASp and thymosin-β4. N-WASp and other Arp-2/3 complex activators need to recruit assembly-competent actin monomers to help in the nucleation process, and ATP monomers are preferred over ADP monomers since they have superior polymerization properties. Similarly, thymosin-β4 plays an important role in sequestering actin monomers, and it would obviously be beneficial to only sequester monomers after they have exchanged their spent ADP nucleotide. These WH2-containing proteins bind to actin in the cleft between subdomains 1 and 3, and the structural changes that we observe in the W-loop would appear to facilitate such discrimination since this region adopts a coil conformation in the ATP state of actin but forms a stable β-sheet in both the ADP-P_i and ADP states. The cocrystal structure of actin and the WH2 domains from WIP, WASp, and N-WASp show the W-loop as a β-sheet in the bound state (12); however, it is impossible for us to know what the encounter complex may look like and whether the

W-loop conformation is a result of binding the WH2 domain. This is an area that needs to be more fully explored in future work.

The conformation of the D-loop has been a point of controversy in the literature. Biochemically, it is clear that differences must exist between the ADP and ATP states since cleavage by subtilisin shows a strong dependence on the nucleotide state (33–35). The ADP and ATP actin crystal structures from the Dominguez lab showed a clear helix in the ADP state, but the D-loop was not able to be resolved in the ATP crystal, indicating it was disordered (16,17). Sablin et al. first suggested that this structural transition could be the result of contacts within the crystal (28), and the recent work by Rould et al. using a nonpolymerizable actin mutant supports this hypothesis (18). In contrast to this most recent study, our simulations show an α-helix in the ADP state and a coil conformation in both the ADP-P_i and ATP states, just as in the TMR-actin structures. Further, we also observe the transition between these helical and coil states upon nucleotide exchange, suggesting that this secondary structure is truly a function of the nucleotide state. There are obvious limitations associated with molecular modeling, primarily the time length of such simulations; however, there are comparable caveats associated with any crystal structure since this is certainly not a natural environment for a protein. It also needs to be emphasized that this helix-coil transition is predicted to be the result of changing a single phosphate group in the nucleotide-binding site. Our simulations were conducted using muscle actin; however, the structures from Rould et al. used an actin gene from *Drosophila* (18). This specific isoform is 93% identical to muscle actin, but contains five potentially important sequence differences in the S-, G-, and H-loops (L-16M, V-17C, I-76V, T-160S, and N-162T). Most of these changes appear to produce small perturbations to the structure; however, N-162 in muscle actin hydrogen bonds with the side chain of either T-277 or T-278, whereas in *Drosophila* T-162 hydrogen bonds with S-281. This change does alter the connectivity in the nucleotide-binding cleft, and given these additional sequence differences in the nucleotide-binding site, the addition or loss of a phosphate group may indeed have an inconsequential effect on the D-loop for this specific actin. This may indicate that the secondary structure of the D-loop is isoform and/or species specific in addition to any dependence on the nucleotide state.

Although we do not observe a secondary structure change in the C-terminal region of actin, we do see a 5-Å shift in the position of the terminal stretch from L-349 to F-375 between the average ADP and ATP states. It is notable that this shift is analogous to the change observed in the cocrystal of actin and profilin (36), suggesting that this may form part of the basis for recognition and nucleotide selectivity by profilin. However since profilin binding induces other large-scale conformational changes in the actin monomer (such as the opening of the nucleotide cleft), it is impossible to separate the thermodynamic contribution of binding from these other conformational changes. This C-terminal helix is also a likely point of contact within the actin filament, and this helix shift coupled with differences in the D-loop conformation could contribute to the differences in polymerization properties of ADP- and ATP-actin. The Holmes F-actin model would support contact in the region (37); however, the recent structure of a cross-linked actin dimer was not able to resolve contacts between subdomains 1 and 2 of the two monomers (38). Much more structural and computational work will be required to further resolve this point.

One of the advantages of molecular simulation is that we can study states that are difficult to access experimentally. One such situation is the ADP-P_i state of actin, and in our simulations we find that this state has characteristics of both of the other nucleotide states. The D-loop is coil in the ADP-P_i state, consistent with the ATP conformation, but the W-loop exactly matches the ADP conformation. Within the nucleotide-binding cleft, the S- and G-loops look the same in all three nucleotide states; however, the H-loop in ADP-P_i-actin exhibits a mix of characteristics, appearing most times like the β-sheet conformation of the ATP state with periodic phases of coil like that observed in the ADP state. The ADP-P_i state is likely only relevant within the filament since dissociation of the phosphate is likely very fast for the monomer in solution, and more extensive F-actin simulations will be required to fully elucidate its properties.

Finally, to examine the nucleotide binding cleft configuration we measured the separation of the D- and G-loops across the binding cleft. Using either the C_α separation of S-14 and G-158 or G-15 and D-157, we see insignificant differences between the three nucleotide states. Our results are in agreement with crystal structures (17,18) and studies using hydroxyl-radical footprinting (39), and we likewise conclude that the nucleotide cleft remains closed in both the ADP and ATP states with no differences in the contacts between subdomains 2 and 4.

SUPPLEMENTARY MATERIAL

To view all of the supplemental files associated with this article, visit www.biophysj.org.

This work was supported by a grant from the National Institutes of Health (GM-067246) to D.S.

REFERENCES

1. De La Cruz, E. M., and T. D. Pollard. 1995. Nucleotide-free actin: stabilization by sucrose and nucleotide binding kinetics. *Biochemistry*. 34:5452–5461.
2. Pollard, T. D., and G. G. Borisy. 2003. Cellular motility driven by assembly and disassembly of actin filaments. *Cell*. 112:453–465.
3. Blanchoin, L., and T. D. Pollard. 2002. Hydrolysis of ATP by polymerized actin depends on the bound divalent cation but not profilin. *Biochemistry*. 41:597–602.

4. Carlier, M. F., and D. Pantaloni. 1986. Direct evidence for ADP-Pi-F-actin as the major intermediate in ATP-actin polymerization. Rate of dissociation of Pi from actin filaments. *Biochemistry*. 25:7789–7792.

5. Belmont, L. D., A. Orlova, D. G. Drubin, and E. H. Egelman. 1999. A change in actin conformation associated with filament instability after Pi release. *Proc. Natl. Acad. Sci. USA*. 96:29–34.

6. Blanchoin, L., T. D. Pollard, and R. D. Mullins. 2000. Interactions of ADF/cofilin, Arp2/3 complex, capping protein and profilin in remodeling of branched actin filament networks. *Curr. Biol.* 10:1273–1282.

7. Ojala, P. J., V. O. Paavilainen, M. K. Vartiainen, R. Tuma, A. G. Weeds, and P. Lappalainen. 2002. The two ADF-H domains of twinfilin play functionally distinct roles in interactions with actin monomers. *Mol. Biol. Cell*. 13:3811–3821.

8. Blanchoin, L., and T. D. Pollard. 1998. Interaction of actin monomers with Acanthamoeba actophorin (ADF/cofilin) and profilin. *J. Biol. Chem.* 273:25106–25111.

9. Vinson, V. K., E. M. De La Cruz, H. N. Higgs, and T. D. Pollard. 1998. Interactions of Acanthamoeba profilin with actin and nucleotides bound to actin. *Biochemistry*. 37:10871–10880.

10. Perelroizen, I., D. Didry, H. Christensen, N. H. Chua, and M. F. Carlier. 1996. Role of nucleotide exchange and hydrolysis in the function of profilin in action assembly. *J. Biol. Chem.* 271:12302–12309.

11. Aguda, A. H., B. Xue, E. Irobi, T. Preat, and R. C. Robinson. 2006. The structural basis of actin interaction with multiple WH2/beta-thymosin motif-containing proteins. *Structure*. 14:469–476.

12. Chereau, D., F. Kerff, P. Graceffa, Z. Grabarek, K. Langsetmo, and R. Dominguez. 2005. Actin-bound structures of Wiskott-Aldrich syndrome protein (WASP)-homology domain 2 and the implications for filament assembly. *Proc. Natl. Acad. Sci. USA*. 102:16644–16649.

13. Mattila, P. K., M. Salminen, T. Yamashiro, and P. Lappalainen. 2003. Mouse MIM, a tissue-specific regulator of cytoskeletal dynamics, interacts with ATP-actin monomers through its C-terminal WH2 domain. *J. Biol. Chem.* 278:8452–8459.

14. Paunola, E., P. K. Mattila, and P. Lappalainen. 2002. WH2 domain: a small, versatile adapter for actin monomers. *FEBS Lett.* 513:92–97.

15. Kabsch, W., H. G. Mannherz, D. Suck, E. F. Pai, and K. C. Holmes. 1990. Atomic-structure of the actin-DNAse-I complex. *Nature*. 347: 37–44.

16. Otterbein, L. R., P. Graceffa, and R. Dominguez. 2001. The crystal structure of uncomplexed actin in the ADP state. *Science*. 293: 708–711.

17. Graceffa, P., and R. Dominguez. 2003. Crystal structure of monomeric actin in the ATP state. Structural basis of nucleotide-dependent actin dynamics. *J. Biol. Chem.* 278:34172–34180.

18. Rould, M. A., Q. Wan, P. B. Joel, S. Lowey, and K. M. Trybus. 2006. Crystal structures of expressed non-polymerizable monomeric actin in the ADP and ATP states. *J. Biol. Chem.* 281:31909–31919.

19. Galkin, V. E., A. Orlova, M. S. VanLoock, A. Shvetsov, E. Reisler, and E. H. Egelman. 2003. ADF/cofilin use an intrinsic mode of F-actin instability to disrupt actin filaments. *J. Cell Biol.* 163:1057–1066.

20. Jacobson, M. P., D. L. Pincus, C. S. Rapp, T. J. Day, B. Honig, D. E. Shaw, and R. A. Friesner. 2004. A hierarchical approach to all-atom protein loop prediction. *Proteins*. 55:351–367.

21. Lindahl, E., B. Hess, and D. van der Spoel. 2001. GROMACS 3.0: a package for molecular simulation and trajectory analysis. *J. Mol. Model*. 7:306–317.

22. Phillips, J. C., R. Braun, W. Wang, J. Gumbart, E. Tajkhorshid, E. Villa, C. Chipot, R. D. Skeel, L. Kale, and K. Schulten. 2005. Scalable molecular dynamics with NAMD. *J. Comput. Chem.* 26:1781–1802.

23. Darden, T., D. York, and L. Pedersen. 1993. Particle mesh Ewald: an N log(N) method for Ewald sums in large systems. *J. Chem. Phys.* 98:10089–10092.

24. MacKerell, A. D., D. Bashford, M. Bellott, R. L. Dunbrack, J. D. Evanseck, M. J. Field, S. Fischer, J. Gao, H. Guo, S. Ha, D. Joseph-McCarthy, L. Kuchnir, K. Kuczera, F. T. K. Lau, C. Mattos, S. Michnick, T. Ngo, D. T. Nguyen, B. Prodhom, W. E. Reiher, B. Roux, M. Schlenkrich, J. C. Smith, R. Stote, J. Straub, M. Watanabe, J. Wiorkiewicz-Kuczera, D. Yin, and M. Karplus. 1998. All-atom empirical potential for molecular modeling and dynamics studies of proteins. *J. Phys. Chem. B*. 102:3586–3616.

25. Jorgensen, W. L., J. Chandrasekhar, J. D. Madura, R. W. Impey, and M. L. Klein. 1983. Comparison of simple potential functions for simulating liquid water. *J. Chem. Phys.* 79:926–935.

26. Evans, D. J., and B. L. Holian. 1985. The Nose-Hoover thermostat. *J. Chem. Phys.* 83:4069–4074.

27. Humphrey, W., A. Dalke, and K. Schulten. 1996. VMD: visual molecular dynamics. *J. Mol. Graph.* 14:33–38.

28. Sablin, E. P., J. F. Dawson, M. S. VanLoock, J. A. Spudich, E. H. Egelman, and R. J. Fletterick. 2002. How does ATP hydrolysis control actin's associations? *Proc. Natl. Acad. Sci. USA*. 99:10945–10947.

29. Marchand, J. B., D. A. Kaiser, T. D. Pollard, and H. N. Higgs. 2001. Interaction of WASP/Scar proteins with actin and vertebrate Arp2/3 complex. *Nat. Cell Biol.* 3:76–82.

30. Vetter, I. R., and A. Wittinghofer. 2001. The guanine nucleotide-binding switch in three dimensions. *Science*. 294:1299–1304.

31. Kudryashov, D. S., and E. Reisler. 2003. Solution properties of tetramethylrhodamine-modified G-actin. *Biophys. J.* 85:2466–2475.

32. Pollard, T. D., L. Blanchoin, and R. D. Mullins. 2000. Molecular mechanisms controlling actin filament dynamics in nonmuscle cells. *Annu. Rev. Biophys. Biomol. Struct.* 29:545–576.

33. Borovikov, Y. S., J. Moraczewska, M. I. Khoroshev, and H. Strzelecka-Golaszewska. 2000. Proteolytic cleavage of actin within the DNase-I-binding loop changes the conformation of F-actin and its sensitivity to myosin binding. *Biochim. Biophys. Acta*. 1478:138–151.

34. Muhlrad, A., P. Cheung, B. C. Phan, C. Miller, and E. Reisler. 1994. Dynamic properties of actin. Structural changes induced by beryllium fluoride. *J. Biol. Chem.* 269:11852–11858.

35. Strzelecka-Golaszewska, H., J. Moraczewska, S. Y. Khaitlina, and M. Mossakowska. 1993. Localization of the tightly bound divalent-cation-dependent and nucleotide-dependent conformation changes in G-actin using limited proteolytic digestion. *Eur. J. Biochem.* 211:731–742.

36. Chik, J. K., U. Lindberg, and C. E. Schutt. 1996. The structure of an open state of beta-actin at 2.65 Å resolution. *J. Mol. Biol.* 263: 607–623.

37. Holmes, K. C., D. Popp, W. Gebhard, and W. Kabsch. 1990. Atomic model of the actin filament. *Nature*. 347:44–49.

38. Kudryashov, D. S., M. R. Sawaya, H. Adisetiyo, T. Norcross, G. Hegyi, E. Reisler, and T. O. Yeates. 2005. The crystal structure of a cross-linked actin dimer suggests a detailed molecular interface in F-actin. *Proc. Natl. Acad. Sci. USA*. 102:13105–13110.

39. Takamoto, K., J. K. Kamal, and M. R. Chance. 2007. Biochemical implications of a three-dimensional model of monomeric actin bound to magnesium-chelated ATP. *Structure*. 15:39–51.